Stable Isotope Labeling−Mass Spectrometry Analysis of Methyl- and Pyridyloxobutyl-Guanine Adducts of 4-(Methylnitrosamino)-1-(3-pyridyl)-1-butanone in *p53*-Derived DNA Sequences†

Mathur Rajesh,‡ Gang Wang,§ Roger Jones,§ and Natalia Tretyakova*,‡,||

University of Minnesota Cancer Center, Minneapolis, Minnesota 55455, Department of Medicinal Chemistry, University of Minnesota School of Pharmacy, Minneapolis, Minnesota 55455, and Department of Chemistry, Rutgers University, Piscataway, New Jersey 08854

Received September 16, 2004; Revised Manuscript Received November 11, 2004

ABSTRACT: The *p53* tumor suppressor gene is a primary target in smoking-induced lung cancer. Interestingly, *p53* mutations observed in lung tumors of smokers are concentrated at guanine bases within endogenously methylated ^{Me}CG dinucleotides, e.g., codons 157, 158, 245, 248, and 273 (^{Me}C = 5-methylcytosine). One possible mechanism for the increased mutagenesis at these sites involves targeted binding of metabolically activated tobacco carcinogens to ^{Me}CG sequences. In the present work, a stable isotope labeling HPLC−ESI$^+$−MS/MS approach was employed to analyze the formation of guanine lesions induced by the tobacco-specific lung carcinogen 4-(methylnitrosamino)-1-(3-pyridyl)-1-butanone (NNK) within DNA duplexes representing *p53* mutational "hot spots" and surrounding sequences. Synthetic DNA duplexes containing *p53* codons 153−159, 243−250, and 269−275 were prepared, where ^{Me}C was incorporated at all physiologically methylated CG sites. In each duplex, one of the guanine bases was replaced with [1,7,-NH_2-$^{15}N_3$-2-^{13}C]-guanine, which served as an isotope "tag" to enable specific quantification of guanine lesions originating from that position. After incubation with NNK diazohydroxides, HPLC−ESI$^+$−MS/MS analysis was used to determine the yields of NNK adducts at the isotopically labeled guanine and at unlabeled guanine bases elsewhere in the sequence. We found that N7-methyl-2′-deoxyguanosine and N7-[4-oxo-4-(3-pyridyl)but-1-yl]guanine lesions were overproduced at the 3′-guanine bases within polypurine runs, while the formation of O^6-methyl-2′-deoxyguanosine and O^6-[4-oxo-4-(3-pyridyl)but-1-yl]-2′-deoxyguanosine adducts was specifically preferred at the 3′-guanine base of 5′-GG and 5′-GGG sequences. In contrast, the presence of 5′-neighboring ^{Me}C inhibited O^6-guanine adduct formation. These results indicate that the N7- and O^6-guanine adducts of NNK are not overproduced at the endogenously methylated CG dinucleotides within the *p53* tumor suppressor gene, suggesting that factors other than NNK adduct formation are responsible for mutagenesis at these sites.

The tobacco-specific nitrosamine 4-(methylnitrosamino)-1-(3-pyridyl)-1-butanone (NNK,[1] Scheme 1) is a systemic pulmonary carcinogen likely to be involved in the initiation of lung cancer in smokers (*1*). Metabolic activation of NNK to DNA-reactive species proceeds by hydroxylation of the carbons adjacent to the *N*-nitroso group, producing methyldiazohydroxide and [4-oxo-4-(3-pyridyl)but-1-yl]diazohydroxide (Scheme 1). DNA alkylation by NNK-derived diazohydroxides gives rise to multiple adducts, including N7-methyl-2′-deoxyguanosine (N7-Me-dG), O^6-methyl-2′-deoxyguanosine (O^6-Me-dG), N7-[4-oxo-4-(3-pyridyl)but-1-yl]-2′-deoxyguanosine (N7-POB-dG), and O^6-[4-oxo-4-(3-pyridyl)but-1-yl]-2′-deoxyguanosine (O^6-POB-dG, Scheme 1) (*2*). While N7-guanine lesions are the most abundant, O^6-substituted guanines are strongly mispairing (*3*). In site-specific mutagenesis studies, both O^6-Me-dG and O^6-POB-dG produced high levels of G → A transition mutations (*4*, *5*), while O^6-POB-dG also led to a small number of G → T transversions (*5*). In addition, O^6-POB-dG adducts are known to inhibit O^6-alkylguanine DNA alkyltransferase (AGT) responsible for the repair of O^6-Me-dG adducts, potentially increasing their persistence *in vivo* (*6*−*8*). In support of the role of these lesions in tobacco mutagenesis, previous studies have observed a correlation between the formation of O^6-Me-dG adducts and lung tumor multiplicity in NNK-treated rats and mice (*9*, *10*). In contrast, N7-Me-dG adducts are not mispairing but can undergo spontaneous depurination

† Funding for this research was provided by a Grant from the National Cancer Institute (CA095039).

* To whom correspondence should be addressed. Telephone: 612-626-3432. Fax: 612-626-5135. E-mail: trety001@umn.edu.

‡ University of Minnesota Cancer Center.

§ Rutgers University.

|| University of Minnesota School of Pharmacy.

[1] Abbreviations: AGT, O^6-alkylguanine-DNA-alkyltransferase; O^6-Me-dG, O^6-methyl-2′-deoxyguanosine; ESI−ITMS, electrospray ionization ion trap mass spectrometry; ESI−MS/MS, electrospray ionization tandem mass spectrometry; ^{Me}C, 5-methylcytosine; MNU, *N*-methyl-*N*-nitrosourea; N7-MeG, N7-methylguanine; N7-POBG, N7-[4-oxo-4-(3-pyridyl)-but-1-yl]guanine; NDMAOAc, *N*-nitroso(acetoxymethyl)-methylamine; NNK, 4-(methylnitrosamino)-1-(3-pyridyl)-1-butanone; NNKOAc, 4-[(acetoxymethyl)-nitrosamino]-1-(3-pyridyl)-1-butanone; O^6-Me-dG, O^6-methyl-2′-deoxyguanosine; O^6-POB-dG, O^6-[4-oxo-4-(3-pyridyl)but-1-yl]deoxyguanosine; POB, pyridyloxobutyl; SPE, solid-phase extraction; SRM, selected reaction monitoring.

10.1021/bi0480032 CCC: $30.25
Published on Web 01/15/2005

Scheme 1: Metabolic Activation of NNK to DNA Reactive Species and the Production of Methylated and Pyridyloxobutylated Guanine Adducts

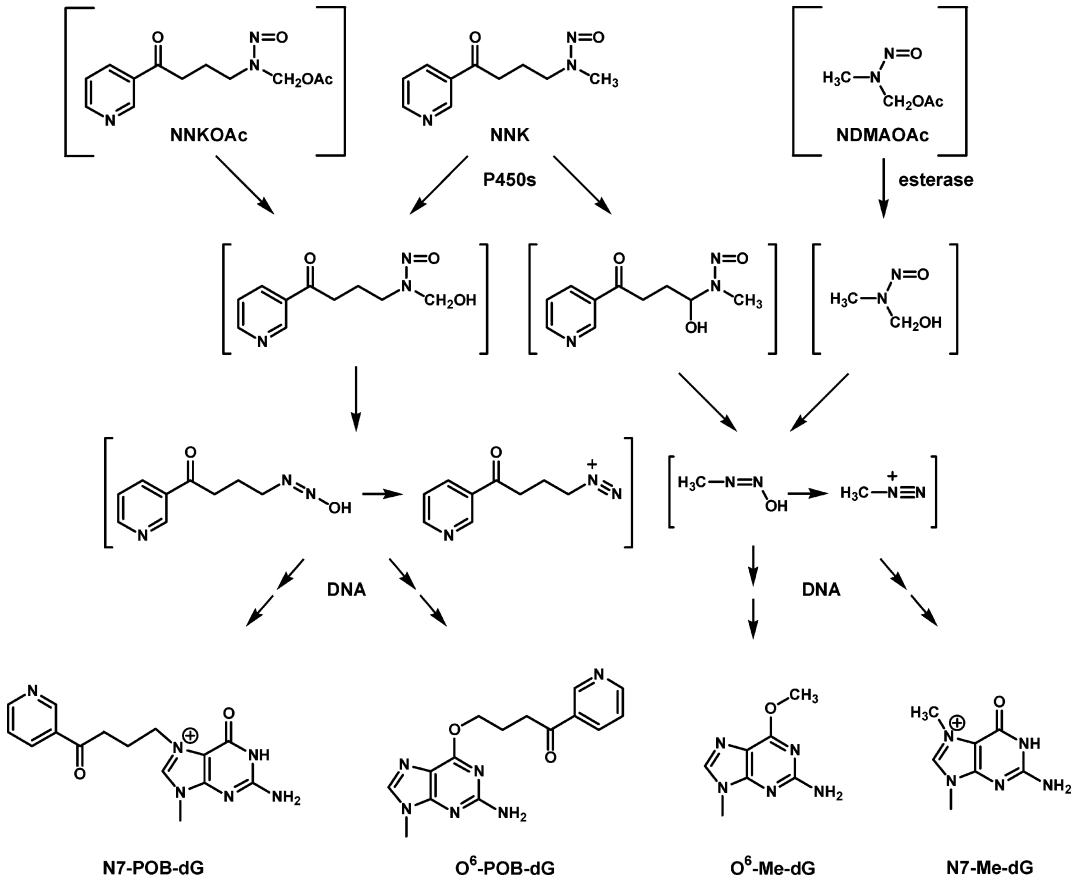

($t_{1/2}$ = 80−160 h) to produce the corresponding free bases and abasic sites in DNA (*3*, *11*). If not repaired, abasic sites can lead to G → T transversions (*12*−*15*).

The *p53* tumor suppressor gene appears to be the major target for genetic damage in smoking-induced cancer (*16*), with approximately 56% of total lung tumors of smokers bearing *p53* mutations (*17*). The *p53* gene encodes a nuclear protein that plays an important role in maintaining genetic integrity. In the presence of DNA damage, p53 protein acts as a transcription factor, up-regulating the expression of several genes involved in cell-cycle control, DNA repair, and apoptosis (*18*, *19*). Increased *p53* expression induces cell-cycle arrest in the late G_1 phase, allowing time for DNA repair and promoting apoptosis of irreversibly damaged cells (*18*, *20*). In cells that have lost normal *p53* function, DNA damage does not trigger up-regulation of *p53*-dependent genes. This allows DNA replication to continue past chemically modified bases without an interruption in cell division, leading to the induction of further genetic damage (*18*, *19*).

The majority of the *p53* base changes observed in lung tumors of smokers are clustered in exons 5, 7, and 8 of the DNA-binding region (*16*). Prominent mutational "hot spots" are observed at codons 157, 158, 245, 248, 249, and 273 (Figure 1) (*17*, *21*). Most of these genetic changes are G → T transversions and G → A transitions occurring at endogenously methylated CG dinucleotides (*22*), with G → T base changes predominating in smokers. While some of these mutations can be rationalized by spontaneous deamination of 5-methylcytosine (^{Me}C) to thymine, the presence of ^{Me}C may also stimulate tobacco carcinogen adduct formation at neighboring guanine bases. For example, cytosine methylation has been shown to increase the yields of guanine adducts induced by diolepoxides of polycyclic aromatic hydrocarbons (*23*), while NNK adduct formation was inhibited in the presence of 5′-neighboring ^{Me}C (*24*).

In the present work, a stable isotope-labeling HPLC−MS/MS method (*25*, *26*) (Scheme 2) was employed to monitor the formation of NNK-induced DNA adducts (N7-Me-dG, O^6-Me-dG, N7-POB-dG, and O^6-POB-dG, Scheme 1) at specific guanine bases within DNA sequences representing the most frequently mutated regions of the *p53* gene. Acetylated precursors of NNK diazohydroxides, *N*-nitroso-(acetoxymethyl)methylamine (NDMAOAc) and 4-[(acetoxymethyl)-nitrosamino]-1-(3-pyridyl)-1-butanone (NNKOAc) (Scheme 1), were employed to model DNA methylation and pyridyloxobutylation by NNK metabolites.

MATERIALS AND METHODS

Warning. NDMAOAc and NNKOAc are carcinogenic and mutagenic in laboratory animals and should be handled with extreme caution (*27*).

Materials. NDMAOAc was purchased from the NCI Chemical Carcinogen Repository (Midwest Research Institute, Kansas City, MO). NNKOAc and N7-[4-oxo-4-(3-pyridyl)but-1-yl]guanine (N7-POBG) were a gift from Professor Stephen Hecht at the University of Minnesota Cancer Center. O^6-POB-dG was a gift from Professor Lisa Peterson at the University of Minnesota Cancer Center. Deuterated methanol was procured from Aldrich Chemical

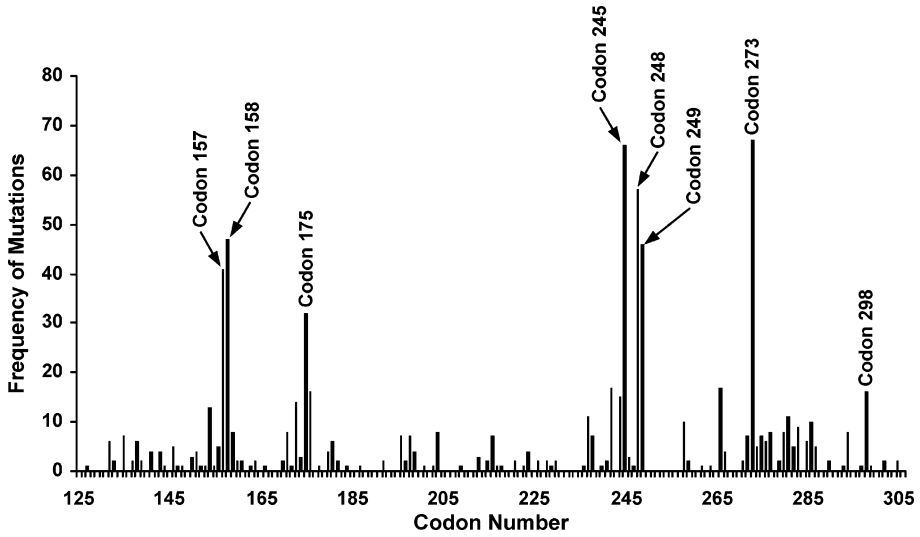

FIGURE 1: Distribution of mutations in human lung cancer mapped along exons 5−8 of the *p53* gene. The frequency of distribution of mutations was obtained from the AACR *p53* mutation database (*22*, *58*). Cancer from nonsmokers and from occupational exposure was excluded.

Scheme 2: Stable Isotope Labeling HPLC−MS Strategy Used to Quantify the Formation of NNK−Guanine Adducts at Specific Guanines within *p53* Gene-Derived DNA Sequences[a]

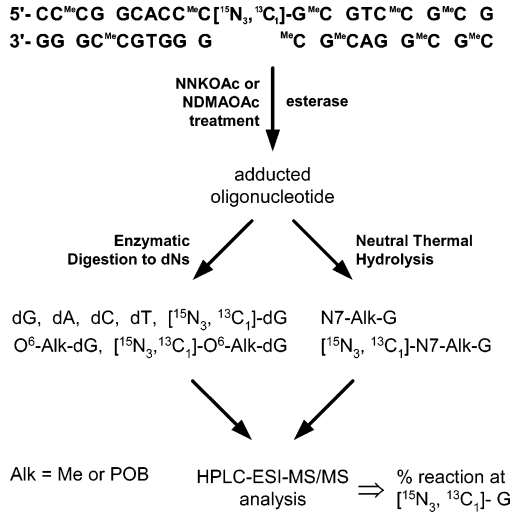

[a] Alk = Me for NDMAOAc-treated DNA or POB for NNKOAc-treated DNA.

Co. (Milwaukee, WI). N7-methylguanine (N7-MeG) and O^6-Me-dG were purchased from Sigma Chemical Co. (St. Louis, MO). [1,7,NH_2-$^{15}N_3$-2-^{13}C]-dG phosphoramidite was prepared at Rutgers University as described elsewhere (*28*). ^{Me}C phosphoramidite was purchased from Glen Research Corp. (Sterling, VA). DNA oligomers containing ^{Me}C and [1,7,-NH_2-$^{15}N_3$-2-^{13}C]-dG at specified locations (Table 1) were prepared by standard phosphoramidite chemistry using a DNA synthesizer at the University of Minnesota Microchemical Facility. In each oligomer, [1,7,NH_2-$^{15}N_3$-2-^{13}C]-dG and ^{Me}C were placed at specified positions as shown in Table 1.

DNase I, phosphodiesterase (PDE) I, PDE II, and micrococcal nuclease were purchased from Worthington Biochemical Corporation (Lakewood, NJ). Porcine esterase and alkaline phosphatase were obtained from Sigma (St. Louis, MO). The deuterated standards D_3-N7-MeG and D_3-O^6-methyl-2′-deoxyguanosine (D_3-O^6-Me-dG) were synthesized as reported previously (*24*). All other chemicals were obtained from general sources and were of the highest grade available.

Selection of DNA Sequences. Double-stranded oligodeoxynucleotides representing *p53* codons 153−159, 243−250, and 269−275 (Table 1) were prepared using standard phosphoramidite methods. These regions of the *p53* gene were selected because they contain known lung-cancer mutational "hot spots" at codons 157, 158, 245, 248, 249, and 273 (Figure 1). ^{Me}C was incorporated in each strand of the duplex at all physiologically methylated CG sites (*29*). In each duplex, one of the guanine bases was replaced with [1,7,NH_2-$^{15}N_3$-2-^{13}C]-dG (Table 1) to allow specific quantification of NNK adducts at that site (see below).

DNA Purification and Purity Control. All DNA oligodeoxynucleotides utilized in this study (Table 1) were purified by semipreparatory HPLC as described previously (*23*). An Agilent Technologies 1100 series HPLC system configured with a binary pump, an autosampler, and either a DAD or VWD UV detector was employed. DNA purity was established by HPLC as reported elsewhere (*24*−*26*). The identity of each DNA strand was confirmed by capillary HPLC−ESI$^-$−MS as previously discussed (*24*−*26*). DNA was considered sufficiently pure for our experiments if the impurity peaks in the HPLC trace constituted less than 2% of the total area.

Quantification of DNA Strands. Quantification of DNA strands was based on HPLC−UV analysis of dG in enzymatic digests of DNA. DNA was dissolved in 10 mM Tris-HCl buffer at pH 7.0 containing 15 mM $MgCl_2$ (180 μM) and hydrolyzed to 2′-deoxynucleosides in the presence of DNase I (30 units/50 μg of DNA), phosphodiesterase I (60 milliunits/50 μg of DNA), and alkaline phosphatase (7.8 units/50 μg of DNA) in 50 mM Tris/15 mM $MgCl_2$ at pH 9.3. At the end of incubation, the digest was dried and the residue was resuspended in 100 μL of water. An aliquot of this solution corresponding to 200−400 pmol of DNA was injected into the HPLC−UV system. A Zorbax Extend-C18 column (4.6 × 150 mm, 5 μm, Aglient Technologies) was eluted at a flow rate of 1 mL/min. The mobile phase consisted of 150 mM ammonium acetate (A) and acetonitrile (B) eluted

Table 1: *p53* Gene-Derived DNA Sequences Selected for This Study

oligonucleotide id	nucleotide number	sequence	calculated molecular weight	observed molecular weight
[$^{15}N_3$,$^{13}C_1$]-*p53*-exon 5-G1,Me2,9,11,14,16	13136−13154	CC^{Me}C[$^{15}N_3$,^{13}C-G]GCACC^{Me}CG^{Me}CGTC^{Me}CG^{Me}CG	5785.7	5785.2
[$^{15}N_3$,$^{13}C_1$]-*p53*-exon 5-G2,Me2,9,11,14,16	13136−13154	CC^{Me}CG[$^{15}N_3$,^{13}C-G]CACC^{Me}CG^{Me}CGTC^{Me}CG^{Me}CG	5785.7	5785.4
[$^{15}N_3$,$^{13}C_1$]-*p53*-exon 5-G3,Me2,9,11,14,16	13136−13154	CC^{Me}CGGCACC^{Me}C[$^{15}N_3$,^{13}C-G]^{Me}CGTC^{Me}CG^{Me}CG	5785.7	5785.0
[$^{15}N_3$,$^{13}C_1$]-*p53*-exon 5-G4,Me2,9,11,14,16	13136−13154	CC^{Me}CGGCACC^{Me}CG^{Me}C[$^{15}N_3$,^{13}C-G]TC^{Me}CG^{Me}CG	5785.7	5785.4
[$^{15}N_3$,$^{13}C_1$]-*p53*-exon 5-G5,Me2,9,11,14,16	13136−13154	CC^{Me}CGGCACC^{Me}CG^{Me}CGTC^{Me}C[$^{15}N_3$,^{13}C-G]^{Me}CG	5785.7	5785.3
(−)*p53*-exon 5,Me1,3,7,9,15		^{Me}CG^{Me}CGGA^{Me}CG^{Me}CGGGTGC^{Me}CGGG	5981.9	5981.8
[$^{15}N_3$,$^{13}C_1$]-*p53*-exon 7-G4,Me6,16	14054−10478	ATGGG^{Me}C[$^{15}N_3$,^{13}C-G]GCATGAAC^{Me}CGGAGGCCCA	7774.1	7773.9
[$^{15}N_3$,$^{13}C_1$]-*p53*-exon 7-G5,Me6,16	14054−10478	ATGGG^{Me}CG[$^{15}N_3$,^{13}C-G]CATGAAC^{Me}CGGAGGCCCA	7774.1	7773.8
[$^{15}N_3$,$^{13}C_1$]-*p53*-exon 7-G6,Me6,16	14054−10478	ATGGG^{Me}CGGCAT[$^{15}N_3$,^{13}C-G]AAC^{Me}CGGAGGCCCA	7774.1	7773.6
[$^{15}N_3$,$^{13}C_1$]-*p53*-exon 7-G7,Me6,16	14054−10478	ATGGG^{Me}CGGCATGAAC^{Me}C[$^{15}N_3$,^{13}C-G]GAGGCCCA	7774.1	7773.8
[$^{15}N_3$,$^{13}C_1$]-*p53*-exon 7-G8,Me6,16	14054−10478	ATGGG^{Me}CGGCATGAAC^{Me}CG[$^{15}N_3$,^{13}C-G]AGGCCCA	7774.1	7773.8
[$^{15}N_3$,$^{13}C_1$]-*p53*-exon 7-G9,Me6,16	14054−10478	ATGGG^{Me}CGGCATGAAC^{Me}CGGA[$^{15}N_3$,^{13}C-G]GCCCA	7774.1	7774.4
(−)*p53*-exon 7,Me9,19		TGGGCCTC^{Me}CGGTTCATGC^{Me}CGCCCAT	7614.0	7614.5
[$^{15}N_3$,$^{13}C_1$]-*p53*-exon 8-G2,Me12	14475−14495	GCTTT[$^{15}N_3$,^{13}C-G]AGGTG^{Me}CGTGTTTGTG	6548.3	6548.1
[$^{15}N_3$,$^{13}C_1$]-*p53*-exon 8-G3,Me12	14475−14495	GCTTTGA[$^{15}N_3$,^{13}C-G]GTG^{Me}CGTGTTTGTG	6548.3	6548.6
[$^{15}N_3$,$^{13}C_1$]-*p53*-exon 8-G4,Me12	14475−14495	GCTTTGAG[$^{15}N_3$,^{13}C-G]TG^{Me}CGTGTTTGTG	6548.3	6549.2
[$^{15}N_3$,$^{13}C_1$]-*p53*-exon 8-G6,Me12	14475−14495	GCTTTGAGGTG^{Me}C[$^{15}N_3$,^{13}C-G]TGTTTGTG	6548.3	6548.5
[$^{15}N_3$,$^{13}C_1$]-*p53*-exon 8-G7,Me12	14475−14495	GCTTTGAGGTG^{Me}CGT[$^{15}N_3$,^{13}C-G]TTTGTG	6548.3	6548.7
(−)*p53*-exon 8,Me9		CACAAACA^{Me}CGCACCTCAAAGC	6336.2	6336.4

using the following gradient: 0−2.5 min, 0% B; 21.5 min, 4.5% B; 24.5−30 min, 30% B; and 33 min, 0% B. UV absorbance was monitored at 260 nm. At these conditions, dG eluted as a sharp peak at 15.5 min. dG amounts in DNA digests were established from HPLC peak areas using calibration curves constructed with 2′-deoxyguanosine standard.

DNA Alkylation and Hydrolysis (Scheme 2). DNA alkylation in the presence of NNK diazohydroxides was conducted as described elsewhere (*24*, *26*). In brief, double-stranded DNA (in quadruplicates, 5 nmol each) was incubated with the alkylating agent (2 mM NDMAOAc or 10 mM NNKOAc) in the presence of porcine esterase (0.11 μg/μL). Previous studies have established that the number of methylated adducts in DNA treated with 2 mM NDMAOAc is ∼5 per 10^3 G (N7-MeG) and ∼5 per 10^4 G (O^6-Me-dG), while the amounts of O^6-POB-dG in DNA treated with 10 mM NNKOAc are 5−6 adducts per 10^5 G (*24*, *26*). The reaction was terminated after 90 min by precipitating the DNA with cold ethanol. The alkylated DNA was dissolved in water and heated to 95 °C for 30 min to release N7-alkylguanine adducts (N7-MeG, N7-POBG, and their [1,7,NH_2-$^{15}N_3$-2-^{13}C] analogues) as free bases. The partially depurinated DNA backbone was precipitated with the addition of cold ethanol. The supernatant was dried under vacuum, and N7-alkylguanine adducts were dissolved in 15 μL of 15 mM ammonium acetate. The sample solution (0.5−4 μL) was injected onto capillary HPLC columns for HPLC−ESI−ITMS analysis as described below (Scheme 2) (*26*).

Following the release of N7-methylguanines from NDMAOAc-treated DNA, ethanol-precipitated DNA pellets were dissolved in 10 mM Tris-HCl buffer at pH 7.0 containing 15 mM $MgCl_2$ and enzymatically hydrolyzed to 2′-deoxynucleosides in the presence of DNase I (30 units/50 μg of DNA), phosphodiesterase I (60 milliunits/50 μg of DNA), and alkaline phosphatase (7.8 units/50 μg of DNA) in 50 mM Tris/15 mM $MgCl_2$ at pH 9.3 buffer. Pyridyloxobutylated DNA was similarly digested in the presence of micrococcal nuclease (1.2 units/50 μg of DNA), phosphodiesterase II (22 milliunits/50 μg of DNA), and alkaline phosphatase (8 units/50 μg of DNA) in 10 mM sodium succinate, 5 mM $CaCl_2$ at pH 6.0 buffer (*26*). Small aliquots of the enzymatic digests (≈1 μL, corresponding to about 160 pmol of DNA) were removed and analyzed by HPLC−UV with the same HPLC method described above for dG analysis to ensure complete enzymatic digestion. O^6-alkyl-dG adducts were isolated by solid-phase extraction (SPE). The samples were loaded onto Strata-X SPE cartridges (Phenomenex, Torrance, CA) and eluted with a step gradient of methanol in water. O^6-Me-dG and O^6-POB-dG adducts eluted in the 50 and 100% methanol fractions, respectively. The solutions were dried under vacuum and redissolved in 15 μL of 15 mM ammonium acetate at pH 5.5. Aliquots (8 μL) of the sample solution were used for capillary HPLC−ESI^+−MS/MS analyses of O^6-Me-dG and O^6-POB-dG as described below.

HPLC−Electrospray Ionization Tandem Mass Spectrometry (ESI−MS/MS) Analyses of Methylated and Pyridyloxobutylated Adducts. All HPLC−ESI−MS/MS experiments were performed with an Agilent Technologies 1100 series capillary HPLC system interfaced to either an Agilent ion trap mass spectrometer (ITMS) or a Finnigan Quantum Discovery triple quadrupole mass spectrometer (TSQ). HPLC analyses of N7-MeG were carried out with a Zorbax SB-C18 column (150 × 0.5 mm, 5 μm, Agilent Technologies) eluted with 15 mM ammonium acetate at pH 5.5 (A) and 100% acetonitrile (B). HPLC column temperature was 20 °C, and the flow rate was 15 μL/min. Mobile phase composition was changed linearly from 5% B to 35% B over the first 16.5 min and further to 40% B over the remaining 2 min. At these conditions, the HPLC retention time of N7-MeG was 5 min. The eluent was introduced into the Agilent ITMS operated in the positive-ion mode. Nitrogen was used

as a drying gas (200 °C, 5 L/min) and as a nebulizing gas (15 psi). The mass spectrometer was operated in the full-scan mode (m/z = 140−180), with target-ion abundance of 30 000 and the maximum accumulation time of 300 ms. Quantitative analyses were performed from reconstructed ion chromatograms of m/z 166 (N7-MeG) and m/z 170 ([1,7,-NH_2-$^{15}N_3$-2-^{13}C]-N7-MeG), $[M + H]^+$.

O^6-Me-dG was analyzed with a Zorbax SB-C18 column (150 × 0.5 mm, 5 μm, Agilent Technologies) eluted with a gradient of 15 mM ammonium acetate at pH 5.5 (A) and 100% acetonitrile (B). Capillary HPLC was carried out at 20 °C at a flow rate of 15 μL/min, with a linear gradient of 0−10.6% B over 15 min, followed by a further increase to 30% B over the next 6 min. At these conditions, O^6-Me-dG eluted at 21 min. The eluent was introduced into the Agilent ITMS operated in the ESI^+−MS/MS mode. Nitrogen was used as a drying gas (200 °C, 5 L/min) and as a nebulizing gas (15 psi). Selected reaction monitoring was performed by monitoring the MS/MS transitions corresponding to the loss of deoxyribose from protonated molecules of O^6-Me-dG (m/z 282.1 $[M + H]^+ \rightarrow$ 166.0 $[M + 2H\text{-dR}]^+$) and [1,7,-NH_2-$^{15}N_3$-2-^{13}C]-O^6-Me-dG (m/z 286.1 $[M + H]^+ \rightarrow$ 170.0 $[M + 2H\text{-dR}]^+$). Target-ion abundance was 30 000, with the maximum accumulation time of 300 ms and the fragmentation amplitude of 0.9 V.

N7-POBG and O^6-POB-dG adducts were analyzed with a Zorbax SB-C18 column (150 × 0.5 mm, 5 μm, Agilent Technologies) eluted with a gradient of 15 mM ammonium acetate (A) and acetonitrile (B). Capillary HPLC was carried out at 25 °C at a flow rate of 15 μL/min, with a linear gradient from 10 to 30% B over 16 min. At these conditions, N7-POBG and O^6-POB-dG eluted at 8.1 and 13.3 min, respectively. The eluent was introduced into the TSQ-MS operated in the ESI^+−MS/MS mode. ESI was achieved at 4000 V, and the capillary temperature was 300 °C. Nitrogen was used as a sheath gas (30 counts). The source CID potential was 8 V, and the tube lens offset voltage was 100 V. MS/MS experiments were performed with the CID gas pressure of 1.5 mTorr (Ar) and CID energy of 30 V. Quantitative analyses of N7-POBG and [1,7,NH_2-$^{15}N_3$-2-^{13}C]-N7-POBG were performed by monitoring the transitions m/z 299.1 $[M + H]^+ \rightarrow$ 148.0 $[POB]^+$ and 152.0 $[Gua + H]^+$ and m/z 303.1 $[M + H]^+ \rightarrow$ 148.0 $[POB]^+$ and 156.0 ([1,7,NH_2-$^{15}N_3$-2-^{13}C]-Gua + H)$^+$, respectively. Quantitative analyses of O^6-POB-dG and [1,7,NH_2-$^{15}N_3$-2-^{13}C]-O^6-POB-dG were performed by monitoring the transitions m/z 415.4 $[M + H]^+ \rightarrow$ 148.0 $[POB]^+$ and 152.0 $[Gua + H]^+$ and m/z 419.4 $[M + H]^+ \rightarrow$ 148.0 $[POB]^+$ and 156.0 ([1,7,NH_2-$^{15}N_3$-2-^{13}C]-Gua + H)$^+$, respectively.

Statistical Analyses of the Data. Statistical analyses were carried out at the University of Minnesota Biostatistics Core. Analysis of variance (ANOVA) (*30*) was used to examine the effects of sequence context on the reactivity at a given guanine base within DNA duplex. F tests were conducted to investigate the effects of the sequence on the formation of adducts at different positions within the same DNA duplex. The pairwise differences in reactivities between two guanine nucleobases were tested using post-hoc t tests, using the formula: $(\mu_1 - \mu_2)/(\text{MSE}(1/n_1 + 1/n_2))^{1/2}$, where μ are the mean reactivities at positions 1 and 2, respectively, and MSE is the mean squared error from the ANOVA analysis. The reactivity of a specific guanine nucleobase was compared with the theoretical "random" reactivity value using the following formula: $(\mu_i - c)/(\text{MSE}(1/n_i))^{1/2}$, where μ_i is the mean reactivity at position i, c is the theoretical reactivity value, and MSE is the mean squared error from ANOVA. To adjust for the number of multiple comparisons and to maintain an overall level of significance at 0.05, p values were adjusted using the Bonferroni method. The Kolmogorov−Smirnov test was used to compare the distributions of different adduct types within a given DNA strand.

RESULTS

Stable Isotope Labeling−HPLC−ESI−MS/MS Approach. The present study utilized the stable isotope labeling-HPLC−ESI−MS/MS approach described previously (*23*−*26*) to map the formation of NNK−guanine adducts within DNA duplexes representing critical regions of the *p53* tumor suppressor gene (Scheme 2). A series of synthetic oligodeoxynucleotides containing *p53* codons 157, 158, 245, 248, and 273 and surrounding sequences were prepared (Table 1). In each duplex, one of the guanine bases was replaced with [1,7,NH_2-$^{15}N_3$-2-^{13}C]-guanine, which served as an isotope "tag" to enable specific quantification of guanine lesions originating from that position (Scheme 2) (*23*−*26*).

Isotopically labeled DNA duplexes were incubated with acetylated precursors of NNK diazohydroxides, NDMAOAc, or NNKOAc, in the presence of esterase (Scheme 2). Neutral thermal hydrolysis was used to release N7-methylguanine and N7-[4-oxo-4-(3-pyridyl)but-1-yl]guanine adducts as free bases. The remaining DNA was then digested enzymatically to recover the O^6-guanine adducts as 2′-deoxynucleosides (Scheme 2). The samples were analyzed by HPLC−ESI^+−MS (N7-MeG) or by HPLC−ESI^+−MS/MS (O^6-Me-dG, O^6-POB-dG, and N7-POBG) to establish the relative extent of adduct formation at the [1,7,NH_2-$^{15}N_3$-2-^{13}C]-labeled and unlabeled nucleobases (Figure 2). Because the molecular weights of the guanine adducts arising from the [1,7,NH_2-$^{15}N_3$-2-^{13}C]-labeled Gua are 4 D higher than those originating from other guanines in the sequence, HPLC−ESI^+−MS/MS can be used to determine the relative extent of adduct formation at the labeled position as follows (Figure 2):

$$\%\ \text{X-dG formation at [1,7,NH}_2\text{-}^{15}\text{N}_3\text{-2-}^{13}\text{C]-dG} = \frac{A_{(\text{X}-[1,7,\text{NH}_2-^{15}\text{N}_3-2-^{13}\text{C}]-\text{dG})}}{A_{(\text{X}-[1,7,\text{NH}_2-^{15}\text{N}_3-2-^{13}\text{C}]-\text{dG})} + A_{\text{X-dG}}} \times 100\%$$

where X is the type of adduct (Me or POB), $A_{(\text{X}-[1,7,\text{NH}_2-^{15}\text{N}_3-2-^{13}\text{C}]-\text{dG})}$ and $A_{\text{X-dG}}$ are the HPLC−ESI−MS peak areas corresponding to [1,7,NH_2-$^{15}N_3$-2-^{13}C]-labeled and unlabeled adducts, respectively (Figure 2). When a set of synthetic oligomers of the same sequence but with a different label position (Table 1) is analyzed, the extent of adduct formation at each site of interest was determined.

Distribution of N7-MeG and O^6-Me-dG Adducts in p53 Exon-5-Derived DNA Sequence (Figure 3). Guanine nucleobases within *p53* codons 157 (***G***TC) and 158 (C***G***C) of exon 5 are frequently mutated in smoking-induced lung cancer (*31*) (Figure 1). To investigate the extent of NNK adduct formation at these sites, a series of stable isotope labeled DNA duplexes representing *p53* codons 153−158 was synthesized (Table 1). ^{Me}C was incorporated in both strands at the five physiologically methylated 5′-CG sites: 5′-

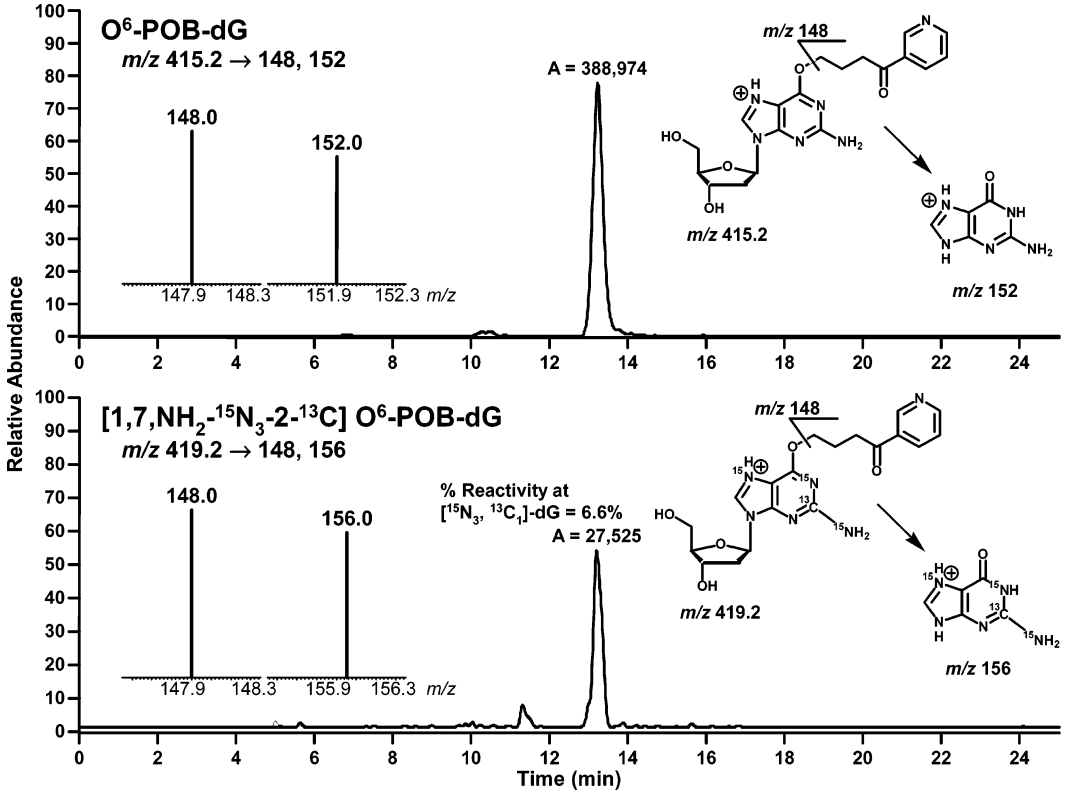

FIGURE 2: Capillary HPLC−ESI$^+$−MS/MS analysis of O^6-POB-dG formed in *p53*-derived DNA duplex [5′-ATGGG^{Me}CGG-CATGAAC^{Me}CG[1,7,NH$_2$-^{15}N$_3$-2-^{13}C]-dGAGGCCCA, (+) strand] following treatment with NNKOAc in the presence of esterase. Upper trace, O^6-POB-dG originating from unlabeled guanine bases; lower trace, [1,7,NH$_2$-^{15}N$_3$-2-^{13}C]-O^6-POB-dG originating specifically from [1,7,NH$_2$-^{15}N$_3$-2-^{13}C]-dG. The quantitative analyses were performed by monitoring for the MS/MS transitions corresponding to the loss of the 2′-deoxyguanosine and deoxyribose + pyridyloxobutyl moiety from the positively charged molecules of the adducts: 415.4 → 148, 152 and 419.4 → 148, 156 for O^6-POB-dG and [1,7,NH$_2$-^{15}N$_3$-2-^{13}C]-O^6-POB-dG, respectively. The extent of reaction at the labeled position was determined from HPLC−ESI$^+$−MS/MS peak areas as follows: % O^6-POB-dG at [1,7,NH$_2$-^{15}N$_3$-2-^{13}C]-dG = $A_{([1,7,NH_2-^{15}N_3-2-^{13}C]-POB-dG)}$/($A_{([1,7,NH_2-^{15}N_3-2-^{13}C]-POB-dG)} + A_{POB-dG}$) × 100%, where $A_{[1,7,NH_2-^{15}N_3-2-^{13}C-POB-dG}$ and A_{POB-dG} are the HPLC−ESI$^+$−MS/MS peak areas corresponding to [1,7,NH$_2$-^{15}N$_3$-2-^{13}C]-labeled and unlabeled adducts, respectively.

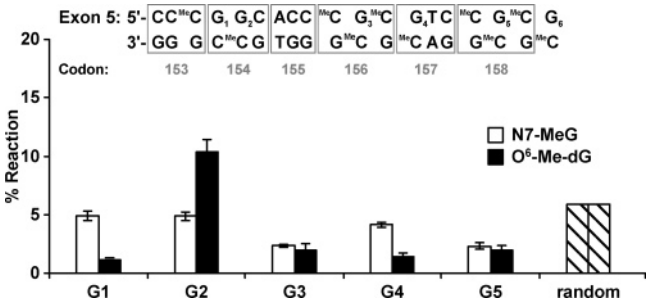

FIGURE 3: Relative formation of N7-MeG (white bars) and O^6-Me-dG adducts (black bars) at guanine nucleobases within a DNA duplex derived from *p53* exon 5 [5′-CC^{Me}C[1,7,NH$_2$-^{15}N$_3$-2-^{13}C]-dGGCACC^{Me}CG^{Me}CGTC^{Me}CG^{Me}CG, (+) strand]. Adduct formation data were compiled from three separate experiments (N = 9−12). The percent of reaction at each guanine was calculated from HPLC−ESI$^+$−MS/MS peak areas as described in the caption to Figure 2. Random reaction value (striped bars) was calculated from the total number of guanine nucleobases in both DNA strands.

CC^{Me}C**G$_1$G$_2$**CACC^{Me}C**G$_3$**^{Me}C**G$_4$**TC^{Me}C**G$_5$**^{Me}CG$_6$ [(+) strand] (Table 1**)** (*29*). [1,7,NH$_2$-^{15}N$_3$-2-^{13}C]-dG was introduced at one of the highlightened positions (**G$_1$**, **G$_2$**, **G$_3$**, **G$_4$**, or **G$_5$**, Table 1). After NMDAOAc treatment and DNA hydrolysis, the relative extent of N7-MeG and O^6-Me-dG formation at [1,7,NH$_2$-^{15}N$_3$-2-^{13}C]-dG was determined by HPLC−ESI$^+$−MS analysis of unlabeled and [1,7,NH$_2$-^{15}N$_3$-2-^{13}C]-labeled adducts (Scheme 2 and Figure 2) (*26*).

In the event of the base sequence not having any effect on the extent of adduct formation, each guanine within the *p53* exon-5-derived duplex would have uniform reactivity of 5.88% per base (100%/17 = 5.88%, where 17 is the total number of guanine nucleobases in this duplex). However, our results demonstrate that the distribution of N7-MeG and O^6-Me-dG adducts in this sequence is not uniform (Figure 3). N7-MeG adduct yields at different guanines follow the order **G$_1$** (^{Me}C***G$_1$***G$_2$) ≈ **G$_2$**(G$_1$***G$_2$***C) > **G$_4$**(^{Me}C***G$_4$***T) > **G$_3$**(^{Me}C***G$_3$***^{Me}C) ≈ **G$_5$**(^{Me}C***G$_5$***^{Me}C) (Figure 3, white bars). N7-MeG adduct formation at **G$_3$**, **G$_4$**, and **G$_5$** (3−4%) is significantly lower than the theoretical value of 5.88% (p < 0.001), while the adduct numbers originating from **G$_1$** and **G$_2$** are within the range of the uniform reaction (p > 0.06) (Figure 3, white bars). N7-MeG amounts originating from **G$_3$** and **G$_5$** are statistically the same (p = 1.0), probably a result of their identical sequence context (^{Me}CG^{Me}C). While N7-MeG adduct yields are low at all five guanine bases tested (Figure 3), somewhat higher reactivity of **G$_1$** and **G$_2$** is consistent with previous reports that alkali-labile adducts of NDMAOAc are overproduced in runs of several Gs (5′-**G$_1$G$_2$**) (*32*).

O^6-Me-dG adduct distribution within the same *p53* exon-5-derived duplex shows a greater variation between different guanines (Figure 3, black bars). Adduct yields follow the order **G$_2$**(G$_1$***G$_2$***C) ≫ **G$_3$**(^{Me}C***G$_3$***^{Me}C) ≈ **G$_5$**(^{Me}C***G$_5$***^{Me}C) > **G$_4$**(^{Me}C***G$_4$***T) > **G$_1$**(^{Me}C***G$_1$***G$_2$). O^6-Me-dG yields at **G$_2$** are

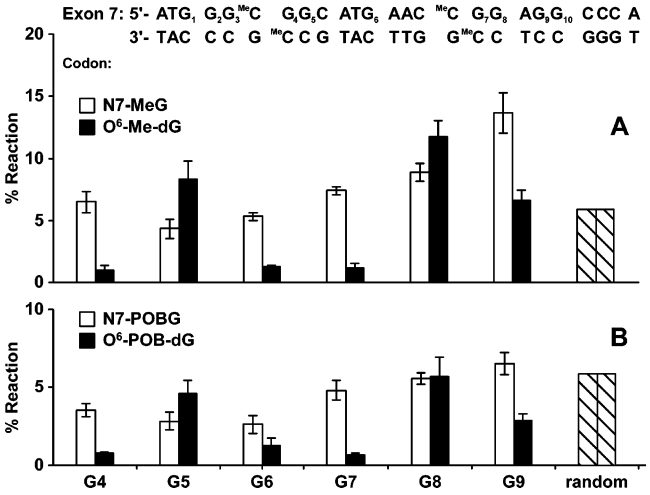

FIGURE 4: Relative formation of N7-MeG (white bars), O^6-Me-dG (black bars) (A), N7-POBG (white bars), and O^6-POB-dG (black bars) (B) at guanine nucleobases within a double-stranded DNA sequence derived from *p53* exon 7 [5′-ATGGG^{Me}-CGGCATGAAC^{Me}CG[1,7,NH$_2$-^{15}N$_3$-2-^{13}C]AGGCCCA, (+) strand]. The adduct formation data were compiled from 2 to 3 separate experiments ($N = 4-12$). Random reaction value (striped bars) was calculated from the total number of guanine nucleobases in both DNA strands. See the caption of Figure 3 for further details.

significantly higher than the theoretical value ($p > 0.0035$), while adduct formation at **G$_1$**, **G$_3$**, **G$_4$**, and **G$_5$** is statistically below the random value ($p < 0.001$). Our observation of low O^6-Me-dG yields at **G$_1$**, **G$_3$**, **G$_4$**, and **G$_5$** (<2%) is consistent with earlier observations that the presence of 5′-neighboring ^{Me}C at these sites decreases total methylation yields and shifts the O^6-Me-dG/N7-MeG molar ratio in favor of N7-alkylation (*24*). In contrast, **G$_2$**, the only guanine in this duplex to be preceded by another guanine (G$_1$***G$_2$***C), gives rise to a higher number of O^6-Me-dG adducts. This result is consistent with our earlier report that the presence of 5′-flanking guanine stimulates the formation of O^6-alkylguanine adducts by NNK diazohydroxides (*26*).

Distribution of N7- and O^6-Methyl Adducts in p53 Exon-7-Derived DNA Sequence (Figure 4A). Base substitution mutations at *p53* exon 7 codons 245 (GGC → TGC), 248 (CGG → CTG), and 249 (AGG → ATG) are characteristic for smoking-associated lung cancer (Figure 1) (*16*). While most of these mutations are G → T transversions, G → A transitions occur with a relatively high frequency at codons 245 (***G***GC → ***A***GC and G***G***C → G***A***C) and 247 (C***G***G → C***A***G) (*16*). To investigate whether any of these sites are targeted for modification by NNK-derived diazohydroxides, a series of double-stranded oligodeoxynucleotides was prepared representing a portion of *p53* sequence containing codons 243−250 (5′-ATG$_1$G$_2$G$_3$^{Me}C**G$_4$G$_5$**CAT**G$_6$**-AAC^{Me}C**G$_7$G$_8$**A**G$_9$**G$_{10}$**CCCA**, where ^{Me}C = 5-methylcytosine) (Table 1). dG was sequentially substituted for [1,7,NH$_2$-^{15}N$_3$,2-^{13}C]-dG at each of the highlighted positions: **G$_4$**, **G$_5$**, **G$_6$**, **G$_7$**, **G$_8$**, and **G$_9$**. ^{Me}C was inserted in both strands at the two endogenously methylated CG sites, 5′-^{Me}C**G$_4$** and 5-^{Me}C**G$_7$** (Table 1). The extent of N7-MeG and O^6-Me-dG adduct formation along this duplex was established from HPLC−MS/MS peak areas corresponding to unlabeled and [1,7,NH$_2$-^{15}N$_3$-2-^{13}C]-labeled adducts as described above (Scheme 2 and Figure 2).

Because the *p53* exon-7-derived duplex contains a total of 17 guanines (Table 1), an unbiased reaction would result in ∼5.9% of adduction occurring at each individual G (100%/17 = 5.88%). However, our results indicate that, with the exception of **G$_4$**, N7-MeG adduct yields at the individual guanine bases are significantly different from the random value ($p < 0.001$). N7-MeG adduct distribution in *p53* exon-7-derived sequence is characterized by a steady increase of reactivity from **G$_5$** toward the 3′ end of the duplex (Figure 4A, white bars). **G$_9$** (G$_7$G$_8$A***G$_9$***G, codon 249) gives rise to the highest number of N7-MeG adducts in this sequence (13.7%), followed by **G$_8$** (G***G$_8$***A, codon 248. 8.9%), **G$_7$** (^{Me}C***G$_7$***G, codon 248, 7.4%), **G$_4$** (^{Me}C***G$_4$***G, codon 245, 6.5%), **G$_6$** (T***G$_6$***A, codon 246, 5.3%), and **G$_5$** (G$_4$***G$_5$***C, codon 245, 4.3%). N7-MeG adduct yields at **G$_5$** (G***G$_5$***C) is below the uniform value ($p < 0.002$). The sites of the highest N7-MeG formation, **G$_9$** (13.7%) and **G$_8$** (8.9%), are located within a polypurine sequence (5′-**G$_7$G$_8$AG$_9$**-3′**)**. This observation is consistent with previous reports that N7-MeG formation is preferred in runs of several purines (*32*).

The pattern of O^6-Me-dG formation within *p53* exon-7-derived duplex is significantly different from that of N7-MeG (Figure 4A, black bars). More pronounced differences between adduct yields at different guanine bases are observed, with a nearly 12-fold variation between the sites of the highest and lowest reactivity (Figure 4A, black bars). The number of adducts originating from **G$_8$** (G***G$_8$***A, 11.7%) is about twice the value expected from random distribution, followed by **G$_5$** (G***G$_5$***C, 8.3%) and **G$_9$** (A***G$_9$***G, 6.4%). In contrast, O^6-Me-dG yields at **G$_4$** (^{Me}C***G$_4$***G**)**, **G$_6$** (T***G$_6$***A), and **G$_7$** (^{Me}C***G$_7$***G) are very poor (<1.3%). The lowest O^6-Me-dG adduct yields are observed at the two endogenously methylated sites, ^{Me}C**G$_4$** and ^{Me}C**G$_7$** (Figure 4A, black bars). In contrast, these same two sites give rise to average numbers of N7-MeG lesions (Figure 4A, white bars). This is consistent with our previous observation that the presence of 5′ flanking ^{Me}C lowers the O^6-Me-dG/N7-MeG molar ratio (*24*). Unlike N7-MeG results (Figure 4A, white bars), O^6-Me-dG formation within the polypurine run 5′-**G$_7$G$_8$**A**G$_9$**-3′ does not show a steady increase from the 5′ to 3′ end but rather hits the highest point at **G$_8$** (Figure 4A, black bars). The presence of an adenine base between **G$_8$** and **G$_9$** alters the distribution pattern for O^6-Me-dG adducts but does not affect the formation of N7-MeG (Figure 4A). The observed distinct differences between O^6-Me-dG and N7-MeG distribution patterns (Figure 4A) are consistent with our earlier results for *K-ras* gene-derived DNA sequences (*26*), further demonstrating that mapping alkali-labile N7-MeG adducts by gel-electrophoresis techniques cannot be used to predict the distribution of promutagenic O^6-Me-dG lesions.

Distribution of N7- and O^6-Methyl Adducts in p53 Exon-8-Derived DNA Sequence (Figure 5). p53 exon 8 hosts a major lung-cancer mutational "hot spot" at codon 273 (^{Me}CGT → ^{Me}CTT) (Figure 1) (*22*). To examine the distribution of O^6-Me-dG and N7-MeG adducts in this critical region of the *p53* gene, a series of synthetic DNA duplexes, 5′-G$_1$-CTTT**G$_2$**A**G$_3$G$_4$**TG$_5$^{Me}C**G$_6$T G$_7$**TTTG$_8$TG$_9$ (+ strand) (Table 1 and Figure 5) were prepared representing *p53* codons 269−275. Stable isotope labeling HPLC−MS/MS (Scheme 2) was employed to quantify the formation of N7- and O^6-methyl adducts at **G$_2$**, **G$_3$**, **G$_4$**, **G$_6$**, and **G$_7$**.

Because the *p53* exon-8-derived duplex contains a total of 11 guanines, sequence-independent methylation would result in ≈9.1% of the adducts forming at each guanine

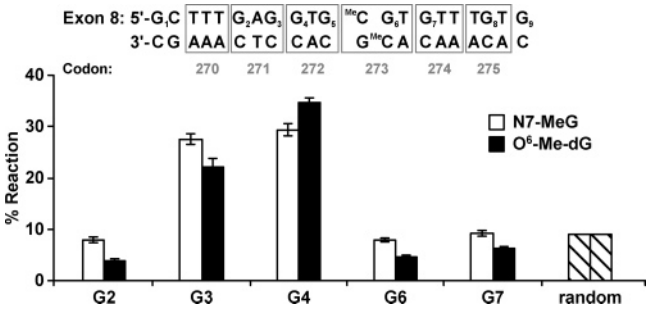

FIGURE 5: Relative formation of N7-MeG (white bars) and O^6-Me-dG (black bars) adducts at guanine nucleobases within a double-stranded DNA sequence derived from *p53* exon 8 [5′-GCTTT[1,7,-NH_2-$^{15}N_3$-2-^{13}C]AGGTG^{Me}CGTGTTTGTG, (+) strand]. Random reaction value (striped bars) was calculated from the total number of guanine nucleobases in both DNA strands. See the caption of Figure 3 for further details.

(100%/11 = 9.09%). We found that while N7-MeG adduct yields at **G2**, **G6**, and **G7** are within the theoretical random value ($p > 0.005$), the reactivities of **G3** (G_2A**G3**, codon 271)- and **G4** (**G4**TG, codon 272) are significantly greater than expected from a random distribution ($p < 0.001$) (Figure 5, white bars). O^6-Me-dG distribution pattern in this sequence is similar to that of N7-MeG, but with more pronounced differences between neighboring guanines (Figure 5, black bars). O^6-Me-dG adduct formation at **G2**, **G6**, and **G7** is below the theoretical random value ($p < 0.001$), while nearly 35% of the total O^6-Me-dG adducts originate from **G4** (***G4***TG, codon 272). This may be explained by the fact that **G4** is the only guanine in this sequence that is preceded by another G (G***G4***T), a factor known to increase the yields of O^6-methylguanine adducts (*26*).

Distribution of N7- and O6-POB Adducts in p53 Exon-7-Derived DNA Sequence (Figure 4B). To determine whether the distribution of guanine adducts induced by POB diazohydroxide within the *p53* gene sequence differs form that generated by Me diazohydroxide, the formation of N7-POBG and O^6-POB-dG adducts was mapped within *p53* exon-7-derived DNA duplex (5′-ATG$_1$G$_2$G$_3$^{Me}C**G4G5**CAT**G6**-AAC^{Me}C**G7G8**A**G9**G$_{10}$CCCA, Table 1). The model pyridyloxobutylating agent, NNKOAc, was used to generate [4-oxo-4-(3-pyridyl)but-1-yl]diazohydroxide in the presence of esterase (Scheme 1).

The patterns of N7-POBG and O^6-POB-dG formation in this sequence were remarkably similar to the distributions of N7-MeG and O^6-Me-dG lesions, respectively (parts A and B of Figure 4). As with the case for N7-MeG, the majority of N7-POBG adducts were formed at **G9** (A**G9**G), while **G8** was the "hot spot" for the formation of both O^6-POB-dG and O^6-Me-dG adducts (Figure 4). The Kolmogorov−Smirnov test comparing the distributions of O^6-Me-dG and O^6-POB-dG adducts within the *p53* exon-7-derived DNA sequence (parts A and B of Figure 4, respectively) fails to reject the null hypothesis, indicating that the distribution patterns of methylated and pyridyloxobutylated adducts of NNK are not significantly different ($p = 0.474$). This is consistent with our previous results comparing the distribution of methyl- and pyridyloxobutyguanine adducts within *K-ras*-derived DNA sequences (*26*). Because methyldiazohydroxide and pyridyloxobutyldiazohydroxide differ significantly in size, this argues against the role of steric factors in determining their sequence selectivity in DNA alkylation.

DISCUSSION

Covalent binding of metabolically activated tobacco carcinogens to DNA nucleobases is considered an early critical step in lung-cancer initiation in smokers (*2*). If not repaired, the resulting DNA adducts can be misread by DNA polymerases, giving rise to irreversible changes in the DNA sequence, which can eventually lead to the induction of lung cancer. In general terms, carcinogen binding to DNA is typically described as the electron transfer from the highest occupied molecular orbital (HOMO) of DNA (nucleophile) to the lowest unoccupied molecular orbital of the carcinogen (electrophile) (*33*). The ability of a particular DNA nucleobase to donate electrons from its HOMO (its ionization potential, IP) can affect its susceptibility to electrophilic attack (*3*, *34*). Among DNA nucleobases, guanine has the lowest IP, making it susceptible to alkylation by electrophilic carcinogens such as NNK-derived diazohydroxides (*35*, *36*). High reactivity of guanine nucleobases toward electrophiles has been corroborated by multiple experimental and theoretical studies of DNA photolysis, photocleavage, oxidation, and alkylation (*3*, *37*−*43*). Importantly, the reactivity of a given guanine toward alkylating agents has been shown to be strongly affected by its sequence context by a combination of electronic, steric, and hydrophobic factors (*44*).

Consistent with known susceptibility of guanine nucleobases toward modification by metabolically activated tobacco carcinogens, the majority of genetic changes observed in smoking-induced lung tumors take place at G:C base pairs. For example, *p53* tumor suppressor gene mutations are primarily G → T transversions at codons 157, 158, 245, 248, and 273 (Figure 1). The formation of these mutational "hot spots" has been proposed to be a result of preferential binding of tobacco carcinogens to guanine nucleobases at these sites (*45*, *46*). Indeed, multiple studies have shown that tobacco carcinogens modify DNA in a highly sequence-selective manner (*23*, *32*, *45*). Therefore, mapping DNA adduct formation by metabolically activated tobacco carcinogen metabolites in the critical regions of the *p53* tumor suppressor gene may provide an insight into the origin of mutational hot spots observed in smoking-induced lung cancer.

Tobacco-specific *N*-nitrosamine, NNK, induces lung tumors in rats, mice, and hamsters (*2*, *11*, *47*, *48*) and is suggested to be involved in the induction of smoking-related pulmonary adenocarcinoma, the leading lung-cancer type in the United States (*2*, *11*, *49*). Several earlier investigations have employed ligation-mediated polymerase chain reaction (LMPCR) to map DNA strand breaks occurring because of the formation of alkali-labile lesions following DNA treatment with methyl- and pyridyloxobutyl diazohydroxides of NNK and other methylating agents (*32*, *50*−*52*). These studies have reported that S_N1-type alkylating agents, e.g., NDMAOAc, *N*-nitroso-*N*-methylurea (MNU) and NNKOAc, preferentially target central guanines within G runs (*32*, *53*). However, an important limitation of these gel-electrophoresis-based techniques is the inability to determine DNA adduct structures. Furthermore, these techniques are limited to alkali-labile adducts and thus cannot detect biologically relevant O^6-guanine adducts of NNK, e.g., O^6-Me-dG and O^6-POB-dG.

The present study was initiated to investigate the formation of O^6- and N7-guanine lesions of NNK in critical regions of

the *p53* tumor suppressor gene (Table 1). Our major goal was to determine the effects of the local sequence context and the presence of 5′-neighboring ^{Me}C on the reactivity of guanine nucleobases within *p53* gene sequence. Our results (Figures 3−5) indicate that NNK-derived methyl- and pyridyloxobutylguanine lesions are produced nonrandomly in all DNA sequences studied. In general, O^6-Me-dG and O^6-POB-dG yields in different sequence contexts follow the order: G***G***A ≈ G***G***C ≈ G***G***T > A***G***G > T***G***T > T***G***A > ^{Me}C***G***A, with the 5′-flanking base being a strong determinant of the extent of O^6-guanine reactivity. O^6-Me-dG and O^6-POB-dG adduct formation is strongly preferred in the presence of a 5′-flanking guanine (Figures 3−5). In contrast, N7-guanine adduct yields follow the order: A***G***G > G***G***A > ^{Me}C***G***G ≫ ^{Me}C***G***G ≈ T***G***A ≈ G***G***C (Figures 3−5). In general, N7-MeG and N7-POBG formation is facilitated at the 3′ end in runs of several purines (Figures 3−5), with a steady increase in the extent of alkylation toward the 3′ end of a polypurine run (Figure 4, white bars). Consistent with this trend, methylating agents frequently induce mutations at the 3′ guanine bases of 5′-GG sequences (*54*). The distribution patterns of pyridyloxobutylated adducts, N7-POBG and O^6-POB-dG, are nearly identical to those of the corresponding methyl adducts (Figure 4), a trend previously observed in *K-ras* gene-derived sequences (*26*). In contrast, the formation of N^2-guanine adducts of benzo[*a*]pyrene diol epoxide within the same *p53* gene-derived DNA duplexes shows very different patterns (*23*), suggesting that different stereoelectronic and hydrophobic factors play a role in determining sequence preferences for DNA modification by reactive metabolites of NNK and benzo[*a*]pyrene.

Guanine bases within runs of several Gs have been previously demonstrated as the preferred sites for oxidation and double-strand scission with direct irradiation and photocleaving agents (*37*, *38*, *40*). Furthermore, central guanines of polyG sequences have been reported to be targeted for N7-methylation by NMDAOAc (*32*). While the exact mechanism of this sequence specificity remains to be established, Wurdeman and collaborators proposed that the reactivity of N7-G sites in polyG sequences toward methyldiazonium ions may be increased as a result of stacking with the 5′-neighboring guanine and the high electrostatic potential at such sequences (*51*). Our results shown here (Figures 3 and 4) are consistent with this rationale, especially because identical results for $CH_3N_2^+$ and $POBN_2^+$ (Figure 4) rule out steric effects as determining factors for the observed sequence selectivity.

The reactivity of the O^6-guanine position toward NNK metabolites is significantly reduced when it is flanked on the 5′ side by a pyrimidine nucleotide, leading to low NNK adduct yields at T***G***T, T***G***A, ^{Me}C***G***G, ^{Me}C***G***T, ^{Me}C***G***T, and ^{Me}C***G***^{Me}C sequences (Figures 3−5). Low O^6-POB-dG and O^6-Me-dG adduct yields in the presence of 5′-flanking ^{Me}C concur with our earlier report that the endogenous methylation at 5′-CG sites reduces O^6-Me-dG and O^6-POB-dG adduct formation (*24*). Because all CG dinucleotides within *p53* exons 5−8 are endogenously methylated to form ^{Me}C (*29*), these sites are expected to be protected against NNK-induced DNA alkylation. Indeed, N7-MeG and O^6-Me-dG adduct yields are low at all ^{Me}CG dinucleotides examined, including known *p53* mutational hot spots at codons 157, 158, 248, and 273 (Figures 3−5). Our results argue against sequence-selective NNK−guanine adduct formation a ^{Me}CG sites, suggesting that factors other than NNK adduct formation are responsible for the observed genetic changes. For example, diolepoxides of polycyclic aromatic hydrocarbons specifically target endogenously methylated ^{Me}CG dinucleotides (*23*, *25*, *46*). Alternatively, these mutations may be rationalized by sequence effects on repair rates (*55*), context-dependent misincorporation during cell replication (*56*), or mutant selection for growth (*57*).

ACKNOWLEDGMENT

We thank Professor Lisa Peterson at the University of Minnesota for the O^6-pyridyloxobutyl-2′-deoxyguanosine standard, Professor Stephen Hecht at the University of Minnesota for the N7-pyridyloxobutylguanine standard and NNKOAc, and Dr. Fangyi Zhao of University of Minnesota Cancer Center Biostatistics Core for her assistance with statistical analyses.

REFERENCES

1. Hecht, S. S., and Hoffmann, D. (1988) Tobacco-specific nitrosamines, an important group of carcinogens in tobacco and tobacco smoke, *Carcinogenesis 9*, 875−884.
2. Hecht, S. S. (1999) DNA adduct formation from tobacco-specific *N*-nitrosamines, *Mutat. Res. 424*, 127−142.
3. Singer, B., and Grunberger, D. (1983) *Molecular Biology of Mutagens and Carcinogens*, Plenum Press, New York.
4. Loechler, E. L., Green, C. L., and Essigmann, J. M. (1984) *In vivo* mutagenesis by O^6-methylguanine built into a unique site in a viral genome, *Proc. Natl. Acad. Sci. U.S.A. 81*, 6271−6275.
5. Pauly, G. T., Peterson, L. A., and Moschel, R. C. (2002) Mutagenesis by O^6-[4-oxo-4-(3-pyridyl)butyl]guanine in *Escherichia coli* and human cells, *Chem. Res. Toxicol. 15*, 165−169.
6. Liu, X. K., Spratt, T. E., Murphy, S. E., and Peterson, L. A. (1996) Pyridyloxobutylation of guanine residues by 4-[(acetoxymethyl)-nitrosamino]-1-(3-pyridyl)-1-butanone generates substrates of O^6-alkylguanine−DNA alkyltransferase, *Chem. Res. Toxicol. 9*, 949−953.
7. Peterson, L. A., Liu, X. K., and Hecht, S. S. (1993) Pyridyloxobutyl DNA adducts inhibit the repair of O^6-methylguanine, *Cancer Res. 53*, 2780−2785.
8. Peterson, L. A., Thomson, N. M., Crankshaw, D. L., Donaldson, E. E., and Kenney, P. J. (2001) Interactions between methylating and pyridyloxobutylating agents in A/J mouse lungs: Implications for 4-(methylnitrosamino)-1-(3-pyridyl)-1-butanone-induced lung tumorigenesis, *Cancer Res. 61*, 5757−5763.
9. Belinsky, S. A., Foley, J. F., White, C. M., Anderson, M. W., and Maronpot, R. R. (1990) Dose−response relationship between O^6-methylguanine formation in Clara cells and induction of pulmonary neoplasia in the rat by 4-(methylnitrosamino)-1-(3-pyridyl)-1-butanone, *Cancer Res. 50*, 3772−3780.
10. Peterson, L. A. and Hecht, S. S. (1991) O^6-methylguanine is a critical determinant of 4-(methylnitrosamino)-1-(3-pyridyl)-1-butanone tumorigenesis in A/J mouse lung, *Cancer Res. 51*, 5557−5564.
11. Hecht, S. S. (1998) Biochemistry, biology, and carcinogenicity of tobacco-specific *N*-nitrosamines, *Chem. Res. Toxicol. 11*, 559−603.
12. Gentil, A., Cabral-Neto, J. B., Mariage-Samson, R., Margot, A., Imbach, J. L., Rayner, B., and Sarasin, A. (1992) Mutagenicity of a unique apurinic/apyrimidinic site in mammalian cells, *J. Mol. Biol. 227*, 981−984.
13. Takeshita, M., and Eisenberg, W. (1994) Mechanism of mutation on DNA templates containing synthetic abasic sites: Study with a double strand vector, *Nucleic Acids Res. 22*, 1897−1902.
14. Avkin, S., Adar, S., Blander, G., and Livneh, Z. (2002) Quantitative measurement of translesion replication in human cells: Evidence for bypass of abasic sites by a replicative DNA polymerase, *Proc. Natl. Acad. Sci. U.S.A. 99*, 3764−3769.
15. Kunkel, T. A. (1984) Mutational specificity of depurination, *Proc. Natl. Acad. Sci. U.S.A. 81*, 1494−1498.

16. Hussain, S. P., Hollstein, M. H., and Harris, C. C. (2000) *p53* tumor suppressor gene: At the crossroads of molecular carcinogenesis, molecular epidemiology, and human risk assessment, *Ann. N.Y. Acad. Sci. 919*, 79−85.
17. Greenblatt, M. S., Bennett, W. P., Hollstein, M., and Harris, C. C. (1994) Mutations in the *p53* tumor suppressor gene: Clues to cancer etiology and molecular pathogenesis, *Cancer Res. 54*, 4855−4878.
18. Harris, C. C. (1996) Structure and function of the *p53* tumor suppressor gene: Clues for rational cancer therapeutic strategies, *J. Natl. Cancer Inst. 88*, 1442−1455.
19. Harris, C. C. (1996) *p53* tumor suppressor gene: From the basic research laboratory to the clinic−An abridged historical perspective, *Carcinogenesis 17*, 1187−1198.
20. Fritsche, M., Haessler, C., and Brandner, G. (1993) Induction of nuclear accumulation of the tumor-suppressor protein p53 by DNA-damaging agents, *Oncogene 8*, 307−318.
21. Hollstein, M., Shomer, B., Greenblatt, M., Soussi, T., Hovig, E., Montesano, R., and Harris, C. C. (1996) Somatic point mutations in the *p53* gene of human tumors and cell lines: Updated compilation, *Nucleic Acids Res. 24*, 141−146.
22. Hernandez-Boussard, T., Rodriguez-Tome, P., Montesano, R., and Hainaut, P. (1999) IARC *p53* mutation database: A relational database to compile and analyze *p53* mutations in human tumors and cell lines. International Agency for Research on Cancer, *Hum. Mutat. 14*, 1−8.
23. Matter, B., Wang, G., Jones, R., and Tretyakova, N. (2004) Formation of diastereomeric benzo[*a*]pyrene diol epoxide−guanine adducts in *p53* gene-derived DNA sequences, *Chem. Res. Toxicol. 17*, 731−741.
24. Ziegel, R., Shallop, A., Upadhyaya, P., Jones, R., and Tretyakova, N. (2004) Endogenous 5-methylcytosine protects neighboring guanines from N7- and O^6-methylation and O^6-pyridyloxobutylation by the tobacco carcinogen 4-(methylnitrosamino)-1-(3-pyridyl)-1-butanone, *Biochemistry 43*, 540−549.
25. Tretyakova, N., Matter, B., Jones, R., and Shallop, A. (2002) Formation of benzo[*a*]pyrene diol epoxide−DNA adducts at specific guanines within *K-ras* and *p53* gene sequences: Stable isotope-labeling mass spectrometry approach, *Biochemistry 41*, 9535−9544.
26. Ziegel, R., Shallop, A., Jones, R., and Tretyakova, N. (2003) *K-ras* gene sequence effects on the formation of 4-(methylnitrosamino)-1-(3-pyridyl)-1-butanone (NNK)−DNA adducts, *Chem. Res. Toxicol. 16*, 541−550.
27. Sansone, E. B., and Tewary, Y. B. (1978) The permeability of laboratory gloves to selected nitrosamines, *IARC Sci. Pub. 19*, 517−529.
28. Shallop, A. J., Gaffney, B. L., and Jones, R. A. (2003) Use of ^{13}C as an indirect tag in ^{15}N specifically labeled nucleosides. Syntheses of [8-^{13}C-1,7,NH_2-$^{15}N_3$]adenosine, -guanosine, and their deoxy analogues, *J. Org. Chem. 68*, 8657−8661.
29. Tornaletti, S., and Pfeifer, G. P. (1995) Complete and tissue-independent methylation of CpG sites in the *p53* gene: Implications for mutations in human cancers, *Oncogene 10*, 1493−1499.
30. Sheskin, D. J. (2000) The between-subjects factorial analysis of variance, in *Handbook of Parametric and Nonparametric Statistical Procedures*, pp 705−755, CRC Press, New York.
31. Hainaut, P., and Pfeifer, G. P. (2001) Patterns of *p53* G → T transversions in lung cancers reflect the primary mutagenic signature of DNA-damage by tobacco smoke, *Carcinogenesis 22*, 367−374.
32. Cloutier, J. F., Drouin, R., and Castonguay, A. (1999) Treatment of human cells with *N*-nitroso(acetoxymethyl)methylamine: Distribution patterns of piperidine-sensitive DNA damage at the nucleotide level of resolution are related to the sequence context, *Chem. Res. Toxicol. 12*, 840−849.
33. Leao, M. B. C., Longo, R. L., and Pavao, A. C. (1999) A molecular orbital analysis of DNA bases, *J. Mol. Struct. 490*, 145−153.
34. Swenson, D. H., and Lawley, P. D. (1978) Alkylation of deoxyribonucleic acid by carcinogens dimethyl sulphate, ethyl methanesulphonate, *N*-ethyl-*N*-nitrosourea and *N*-methyl-*N*-nitrosourea. Relative reactivity of the phosphodiester site thymidylyl-(3′-5′)thymidine, *Biochem. J. 171*, 575−587.
35. Fernando, H., Papadantonakis, G. A., Kim, N. S., and LeBreton, P. R. (1997) The energetics of nucleotide ionization in water counterion environments, in *Molecular Modeling of Nucleic Acids, ACS Symposium Series* (Leontis, N., and SantaLucia, J. J., Eds.) pp 18−40, Washington, D.C.
36. Orlov, V. M., Smirnov, A. N., and Varshavsky, Y. M. (1976) Ionization potentials and electron-donor ability of nucleic acid bases and their analogs, *Tetrahedron Lett. 48*, 4377−4378.
37. Saito, I., Takayama, M., Sugiyama, H., Nakatani, K., Tsuchida, A., and Yamamoto, M. (1995) Photoinduced DNA cleavage via electron transfer: Demonstration that guanine residues located 5′ to guanine are the most electron-donating sites, *J. Am. Chem. Soc. 117*, 6406−6407.
38. Sugiyama, H., and Saito, I. (1996) Theoretical studies of GG-specific photocleavage of DNA via electron transfer: Significant lowering of ionization potential and 5′-localization of HOMO of stacked G bases in B-form DNA, *J. Am. Chem. Soc. 118*, 7063−7068.
39. Saito, I., Nakamura, T., and Nakatani, K. (2000) Mapping of highest occupied molecular orbitals of duplex DNA by cobalt-mediated guanine oxidation, *J. Am. Chem. Soc. 122*, 3001−3006.
40. Saito, I., Nakamura, T., Nakatani, K., Yoshioka, Y., Yamaguchi, K., and Sugiyama, H. (1998) Mapping of the hot spots for DNA damage by one-electron oxidation: Efficacy of GG doublets and GGG triplets as a trap in long-range hole migration, *J. Am. Chem. Soc. 120*, 12686−12687.
41. Yoshioka, Y., Kitagawa, Y., Takano, Y., Yamaguchi, K., Nakamura, T., and Saito, I. (1999) Experimental and theoretical studies on the selectivity of GGG triplets toward one-electron oxidation in B-form DNA, *J. Am. Chem. Soc. 121*, 8712−8719.
42. Prat, F., Houk, K. N., and Foote, C. S. (1998) Effect of guanine stacking on the oxidation of 8-oxoguanine in B-DNA, *J. Am. Chem. Soc. 120*, 845−846.
43. Kim, N. S., Zhu, Q., and LeBreton, P. R. (1999) Aqueous ionization and electron-donating properties of dinucleotides: Sequence-specific electronic effects on DNA alkylation, *J. Am. Chem. Soc. 121*, 11516−11530.
44. Warpehoski, M. A., and Hurley, L. H. (1988) Sequence selectivity of DNA covalent modification, *Chem. Res. Toxicol. 1*, 315−333.
45. Denissenko, M. F., Pao, A., Tang, M., and Pfeifer, G. P. (1996) Preferential formation of benzo[*a*]pyrene adducts at lung cancer mutational hotspots in *p53*, *Science 274*, 430−432.
46. Denissenko, M. F., Chen, J. X., Tang, M. S., and Pfeifer, G. P. (1997) Cytosine methylation determines hot spots of DNA damage in the human *p53* gene, *Proc. Natl. Acad. Sci. U.S.A. 94*, 3893−3898.
47. Hecht, S. S., Chen, C. B., Ohmori, T., and Hoffmann, D. (1980) Comparative carcinogenicity in F344 rats of the tobacco-specific nitrosamines, *N*′-nitrosonornicotine and 4-(*N*-methyl-*N*-nitrosamino)-1-(3-pyridyl)-1-butanone, *Cancer Res. 40*, 298−302.
48. Hecht, S. S. (1999) Tobacco smoke carcinogens and lung cancer, *J. Natl. Cancer Inst. 91*, 1194−1210.
49. Thun, M. J., Lally, C. A., Flannery, J. T., Calle, E. E., Flanders, W. D., and Heath, C. W., Jr. (1997) Cigarette smoking and changes in the histopathology of lung cancer, *J. Natl. Cancer Inst. 89*, 1580−1586.
50. Cloutier, J. F., Drouin, R., Weinfeld, M., O'Connor, T. R., and Castonguay, A. (2001) Characterization and mapping of DNA damage induced by reactive metabolites of 4-(methylnitrosamino)-1-(3-pyridyl)-1-butanone (NNK) at nucleotide resolution in human genomic DNA, *J Mol. Biol. 313*, 539−557.
51. Wurdeman, R. L., and Gold, B. (1988) The effect of DNA sequence, ionic strength, and cationic DNA affinity binders on the methylation of DNA by *N*-methyl-*N*-nitrosourea, *Chem. Res. Toxicol. 1*, 146−147.
52. Shoukry, S., Anderson, M. W., and Glickman, B. W. (1993) Use of fluorescently tagged DNA and an automated DNA sequencer for the comparison of the sequence selectivity of SN1 and SN2 alkylating agents, *Carcinogenesis 14*, 155−157.
53. Cloutier, J. F., Castonguay, A., O'Connor, T. R., and Drouin, R. (2001) Alkylating agent and chromatin structure determine sequence context-dependent formation of alkylpurines, *J. Mol. Biol. 306*, 169−188.
54. Sukumar, S., Notario, V., Martin-Zanca, D., and Barbacid, M. (1983) Induction of mammary carcinomas in rats by nitroso-methylurea involves malignant activation of H-ras-1 locus by single point mutations, *Nature 306*, 658−661.
55. Delaney, J. C., and Essigmann, J. M. (2001) Effect of sequence context on O^6-methylguanine repair and replication *in vivo*, *Biochemistry 40*, 14968−14975.
56. Page, J. E., Zajc, B., Oh-hara, T., Lakshman, M. K., Sayer, J. M., Jerina, D. M., and Dipple, A. (1998) Sequence context profoundly

influences the mutagenic potency of trans-opened benzo[*a*]pyrene 7,8-diol 9,10-epoxide-purine nucleoside adducts in site-specific mutation studies, *Biochemistry 37*, 9127−9137.
57. Rodin, S. N., and Rodin, A. S. (2000) Human lung cancer and *p53*: The interplay between mutagenesis and selection, *Proc. Natl. Acad. Sci. U.S.A. 97*, 12244−12249.
58. Hernandez-Boussard, T. M., and Hainaut, P. (1998) A specific spectrum of *p53* mutations in lung cancer from smokers: Review of mutations compiled in the IARC *p53* database, *Environ. Health Perspect. 106*, 385−391.

BI0480032